AIP Advances

Brewster angle optical reflection observation of self-limiting nanoparticle monolayer self-assembly at a liquid/liquid interface

Cite as: AIP Advances **9**, 065022 (2019); https://doi.org/10.1063/1.5099487
Submitted: 10 April 2019 • Accepted: 19 June 2019 • Published Online: 26 June 2019

Jiayang Hu, Brady Pan, Takuma Makihara, et al.

ARTICLES YOU MAY BE INTERESTED IN

Experimental and numerical study on the drainage performance and fluid flow of Venturi tubes
AIP Advances **9**, 065003 (2019); https://doi.org/10.1063/1.5099420

Nanofocusing on gold planar nanotip arrays
AIP Advances **9**, 065103 (2019); https://doi.org/10.1063/1.5093469

A fuzzy artificial neural network-based method for Cerenkov luminescence tomography
AIP Advances **9**, 065105 (2019); https://doi.org/10.1063/1.5088234

AIP Advances ARTICLE scitation.org/journal/adv

Brewster angle optical reflection observation of self-limiting nanoparticle monolayer self-assembly at a liquid/liquid interface

Cite as: AIP Advances 9, 065022 (2019); doi: 10.1063/1.5099487
Submitted: 10 April 2019 • Accepted: 19 June 2019 •
Published Online: 26 June 2019

View Online Export Citation CrossMark

Jiayang Hu,[1,a)] Brady Pan,[1,a)] Takuma Makihara,[1,b)] Roy D. J. Garcia,[1] and Irving P. Herman[1,c)]

AFFILIATIONS

[1] Department of Applied Physics and Applied Mathematics, Columbia University, New York, New York 10027, USA

[a)] The first two authors contributed equally.
[b)] Also with Department of Physics and Astronomy, Rice University, Houston, Texas 77251, USA.
[c)] **E-mail:** Corresponding author, iph1@columbia.edu

ABSTRACT

Real-time optical reflection of incident *p*-polarized light near Brewster's angle shows that after drop-casting iron oxide nanoparticles (NPs) in heptane on top of a diethylene glycol (DEG) liquid substrate, an iron oxide NP layer forms at the DEG/heptane interface, and it self-limits to a monolayer even when there are excess NPs dispersed in the upper heptane phase. Most modes of NP self-assembly do not self-limit growth after the formation of a single monolayer. Observations are compared to a reflection model incorporating the reflectances expected at each interface. An effective medium model of the dielectric constant is used to model the reflectance of the NP layer at the DEG/heptane interface.

I. INTRODUCTION

One way of forming nanostructures is by the self-assembly of nanoparticles (NPs) at a liquid surface, followed by transfer of the NP layer to another surface.[1–5] After NPs dispersed in a solvent are drop-cast on a denser, less volatile, and immiscible lower solvent, the number of NP layers remaining on the lower solvent after the upper one has evaporated depends on the number of NPs deposited during drop-casting.[4,5] This standard assembly method may lead to a NP monolayer (ML), as may be desired,[5] only for carefully calibrated numbers of drop-cast NPs. The NP layer can self-limit to a ML if the solvents are miscible, but this is not always possible or desirable.[5] By using optical reflection monitoring near Brewster's angle, we show that when an iron oxide NP heptane colloid or dispersion is drop-cast on a diethylene glycol (DEG) liquid substrate, an example of the general route using immiscible solvents, a NP layer forms at the liquid/liquid interface before the upper solvent evaporates. Moreover, this layer is limited to a ML. Earlier experimental and modeling studies suggested that all of the drop-cast iron oxide NPs remained in the upper solvent before it evaporated.[4,6–8]

The Pieranski model[6] has been used to explain the binding of particles at interfaces, and has been used to account for the long-known Pickering effect, the sometimes unexpected stability of bubbles and emulsions.[9] However, the binding of particles to liquid/liquid interfaces relative to the thermal energy decreases rapidly with particle size, so it is not certain whether or not NPs will bind stably to many interfaces.[10] For the system under study, this model predicts it is energetically favorable for the oleate-capped iron oxide NPs to remain in the heptane solvent over binding to the DEG/heptane interface, as noted, but there are uncertainties in the model parameters and in the importance of higher order binding effects that may explain the differences between experiment and simple modeling.[4] Determining whether such binding can occur for this system is one motivation for this study.

Brewster angle reflectometry is known to be sensitive to even Angstrom-level thick materials at interfaces and surfaces.[11,12] Previously, optical probes of NP MLs on liquid surfaces and interfaces did not need this sensitivity because metal NPs were being probed, as in the use of UV/VIS absorption[13] and of reflectance and transmission at normal incidence,[14] and of reflectance near the critical angle of the interface.[15] However, given the relatively small mismatches of oxide nanoparticle and organic liquid refractive indices, it is not clear how effective Brewster angle reflectometry would be in monitoring oxide NPs at such liquid/liquid interfaces and what could be learned from such probing. Exploring whether or not this probe can be a valuable real-time optical diagnostic of this self-assembly process is a second motivation for this study.

II. EXPERIMENTAL METHODS

To form these NP assemblies, 2 mL of DEG were first deposited into a glass Petri dish (diameter = 3.45 cm) to form a ~2.14 mm-thick liquid substrate (if the surface were flat). A *p*-polarized He-Ne laser (632.8 nm, plasma filter) was expanded from below to form a 2.21 cm × 1.32 cm elliptical beam at the center of the DEG/air interface, to average over this region, and all reflected beams other than those from the glass bottom of the Petri dish were imaged on a photodiode, on which they overlap (Fig. 1). The laser was adjusted to hit the DEG/air interface at Brewster's angle (34.65°) to minimize reflectance from this interface. Then, 1400 μL of heptane were deposited on the DEG substrate to form a ~1.50 mm-thick upper layer reservoir and, finally, 120 μL of a heptane colloid of NPs were drop-cast on top. This quickly mixed with the heptane reservoir to form a more dilute, ~1.63 mm-thick heptane colloid layer. The Petri dish was then capped to slow the heptane evaporation. The NPs were spherical iron oxide NPs (Fe_2O_3, 11.8 nm core diameter, capped by oleate) synthesized by standard methods.[16] The number of NPs in the heptane colloid drop was characterized by the number of close-packed NP MLs that would be expected to form on the DEG substrate after heptane evaporation, averaged over the surface; this is termed the number of ML-equivalents being drop-cast.

The light beams reflected from the DEG/heptane colloid and heptane colloid/air interfaces were monitored by a photodiode for 240 min, way before the heptane upper layer evaporated. Before the heptane was added, the reflected fraction from the DEG/air interface was very small, but not zero, because of the surface and laser beam curvatures. After it was added and before the NPs were drop-cast, the reflectances from the DEG/heptane and heptane/air interfaces were still very small because the refractive indices of pure DEG and heptane are nearly the same (below). After the NPs were added and a NP layer formed at the DEG/heptane colloid interface, the reflectance from that interface was expected to initially increase monotonically and linearly with layer thickness at the interface (for up to ~6 MLs, corresponding to ~ a quarter wavelength in this medium).

III. RESULTS AND DISCUSSION

Figure 2 shows the monitored reflected signal was initially very small and then after drop-casting 1, 3, 6, 9, 15, or 18 ML-equivalents

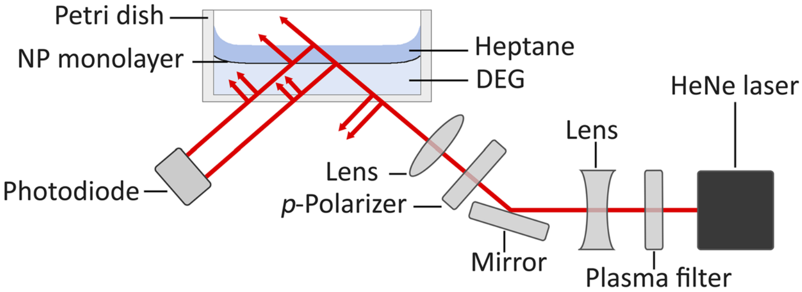

FIG. 1. Experimental schematic.

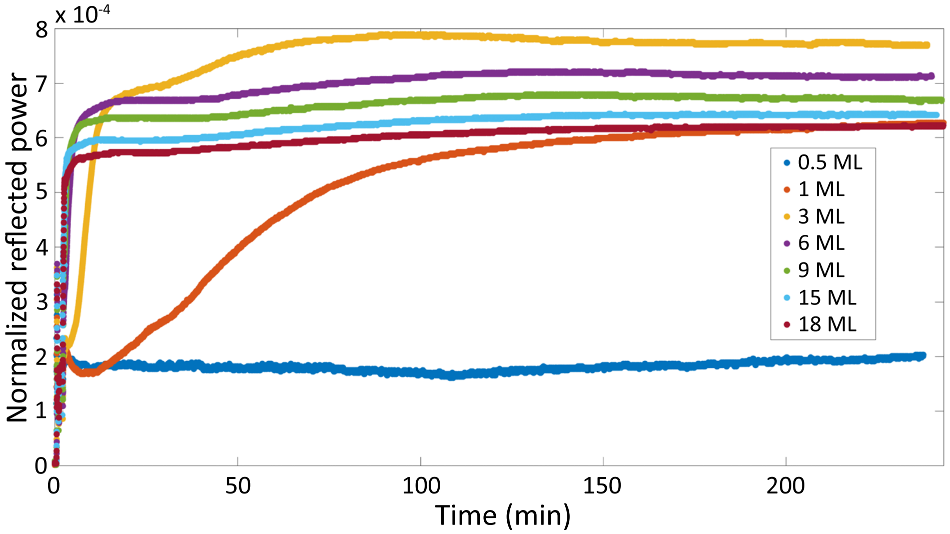

FIG. 2. Traces of monitored reflected light after the NP colloid was drop-cast, for different numbers of NP ML-equivalents drop-cast, normalized by laser power incident on the Petri dish.

of NPs, the reflected signal increased due to the arrival and assembly of NPs at the DEG/heptane interface. In steady state, the reflected signal was roughly the same over this range. This is consistent with the formation of 1 ML of NPs at the liquid/liquid interface in each case, with the remainder of the NPs staying in the heptane colloid. When 1 ML of NPs were drop-cast, the steady-state reflected signal was a little smaller than when 3 ML were drop-cast, perhaps due to inhomogeneities in the NP layer. Furthermore, there was a small monotonic decrease in the steady-state signal as the number of NP MLs drop-cast was increased from 3 to 18. The time needed to reach steady state decreased with the number of ML-equivalents drop-cast, as is expected due to the larger flux of NPs to the liquid/liquid interface. No change in reflectance was seen after 0.5 ML of NPs were drop-cast, perhaps due to the assembly process or inhomogeneities on the surface. The reflectances for a second series of runs conducted with several more tests with 3 and fewer ML-equivalents of NPs drop-cast are shown in Fig. S1 in the supplementary material. These observations are consistent with what is seen in Fig. 2, with a seemingly nonlinear variation of reflectance when the number of ML-equivalents drop-cast is increased from 0 to ~1 ML.

In the reflection model, the reflectance at the DEG/NP ML/heptane colloid interface is determined by the standard three-medium model in optics, while that at the heptane colloid/air interface is obtained from the two-medium model.[17] To compare with experiments, the power of the laser beam entering the Petri dish is tracked in the model as it enters the dish, encounters reflections at all interfaces and the surface, and then leaves the dish; this includes potential absorption in the heptane colloid, which was directly measured in separate experiments. The signals on the photodiode in the experiment and model include reflections at the heptane/NP ML/heptane colloid and the heptane colloid/air interfaces, which simply add because there is no interference.

The refractive index, $n + ik$, of each medium containing NPs is obtained using dielectric constants at the probe wavelength determined by effective medium models, with $\epsilon_{eff} = (n + ik)^2$. ϵ_{eff} for the NP ML at the DEG/heptane interface is obtained using the Bruggeman effective medium model:[18,19]

$$f\,\frac{\epsilon_{NP}-\epsilon_{eff}}{\epsilon_{NP}+2\epsilon_{eff}}+(1-f)\,\frac{\epsilon_{liquid}-\epsilon_{eff}}{\epsilon_{liquid}+2\epsilon_{eff}}=0. \tag{1}$$

or the Maxwell-Garnett effective medium model:[17,18]

$$\epsilon_{eff}=\epsilon_{liquid}\,\frac{\epsilon_{NP}+2\epsilon_{liquid}+2f\left(\epsilon_{NP}-\epsilon_{liquid}\right)}{\epsilon_{NP}+2\epsilon_{liquid}-f\left(\epsilon_{NP}-\epsilon_{liquid}\right)}. \tag{2}$$

For this 1 ML of close-packed NPs, f is the volume fraction of the iron oxide NP cores, which have dielectric constant ϵ_{NP}. The mixture of heptane and DEG (and ligands) within this ML has dielectric constant ϵ_{liquid}. The core-core distance of the 2D close-packed hexagonal (11.8 nm-diameter) cores capped by ligands is taken to be 14.7 nm (as measured in small-angle x-ray scattering (SAXS) studies[20]) and the ML thickness is taken to be 15.8 nm (diameter of the NP with fully extended ligands). The heptane colloid is modeled using either the Bruggeman model or Maxwell Garnett effective medium model,[18,19] for which the liquid in the model is heptane.

The refractive indices of the bulk materials used in the reflection and effective medium models at 632.8 nm are $n_{\text{heptane}} = 1.3875$,[21] $n_{\text{DEG}} = 1.4462$ (estimated using the DEG value at 589 nm and the values for ethylene glycol at 589 nm[22–24] and 632.8 nm[23,24]), and $n_{\text{Fe2O3}} = 3.1258 + 0.070760i$.[25] The refractive index of the ligands is assumed to be that of the solvent it displaces in the ML model. The uncertainty in using bulk values in the refractive index contribution of the NP cores to the heptane colloid refractive index does not affect the interface and surface reflectances because the heptane colloid is so dilute that it can be treated as pure heptane, as is seen below, but it did affect tracking beam absorption in the heptane colloid between the liquid/liquid interface and the upper surface. Consequently, absorption in a cuvette was directly measured, across 1 cm of NP colloids with concentrations that corresponded to heptane colloids for 2, 5, 8, 14, and 17 ML-equivalents in the Petri dish, assuming that 1 ML had been removed from the colloid and was at the liquid/liquid interface, and this is used in the model.

Because the exact vertical location of the NP ML at the DEG/heptane interface is uncertain, two bounds are calculated, assuming that the NP cores were essentially either in the DEG or in the heptane layer, so the liquid at the interface is chosen to be either DEG or heptane in the effective medium models. These give a real part of the effective index of refraction for the NP ML of 1.8676 and 1.8187 in the Bruggeman model, respectively with DEG or heptane, and of 1.8134 and 1.7574 in the Maxwell-Garnett model. The model that assumes the NPs are essentially in heptane is probably better because the Pieranski model[4,6–8] suggests the NPs remain dispersed in the heptane layer and the NP ligands are more soluble in heptane than in DEG.

Figure 3 compares the experimental reflected fraction from Fig. 2 at 240 min, which is the ratio of the laser power leaving the Petri dish to that entering it, with corresponding model predictions for this total, reflected fraction and the reflectances at the DEG/heptane colloid and heptane colloid/air interfaces (with the Maxwell-Garnett model of the colloid). In Fig. 3, the reflection model predictions using for the Maxwell-Garnett effective medium model for the DEG/heptane liquid interface with the NPs in the ML bathed in heptane are plotted vs. the number of ML-equivalents drop-cast.

Comparison of the experimental reflected fraction with the broader set of model predictions is made in Fig. S2 in the supplementary material, with the model reflected fractions plotted for the interfacial NPs either in the heptane or DEG, and using either the Bruggeman, Maxwell Garnett, or simple volume fraction model for the interface. The reflected fraction predictions are larger assuming the NPs are in the (higher refractive index) DEG than in heptane, as expected, and are the largest for the volume fraction model, smaller for the Bruggeman model, and smallest for the Maxwell-Garnett model. The smallest reflected fraction in Fig. S2, that for NPs in heptane in the Maxwell-Garnett model as is also plotted in Fig. 3, is closest to observations and is expected to be the most realistic model because the NPs are indeed mostly in heptane and the Maxwell-Garnett model assumes spheres (the NP cores here) within a uniform medium (a sea of liquid here).

The change in the interface and surface reflectances due to the presence of the NPs remaining in the colloid after NP layer formation (1 ML-equivalent less than that drop-cast) is negligible for both effective medium models of the colloid, and so for this the colloids can be treated as pure liquids. However, the decreased transmission in the colloids due to NP absorption is significant in the model

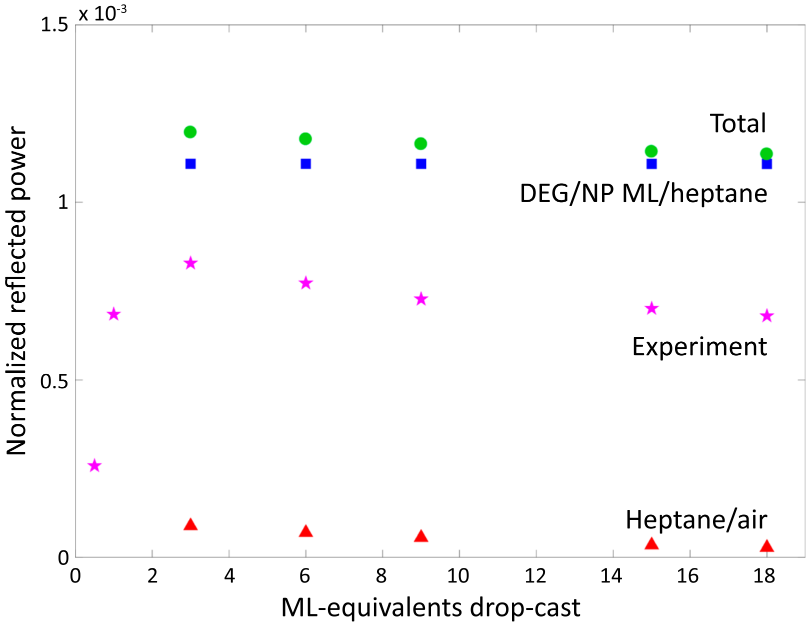

FIG. 3. Reflected power fraction (that leaving the Petri dish and monitored, normalized by the power incident on it) from the experiment (pink stars) shown in Fig. 2 (at 240 min) and the model vs. different numbers of NP ML-equivalents drop-cast. The model ("total") reflected signal assumes 1 ML-equivalent is at the DEG/heptane colloid interface (Maxwell-Garnett model), essentially in the heptane colloid, (green circles) and the remaining NPs are in the heptane colloid (modelled by the Maxwell-Garnett model). The calculated reflectance at the DEG/NP ML/heptane colloid interface is plotted assuming the NP ML is again essentially in the heptane colloid (blue squares). The model reflectance at the heptane colloid/air interface is also shown (red triangles). Fig. S2 in the supplementary material presents the model reflectance for other dielectric function models and locations of the NPs near the DEG/heptane interface.

of the total reflected fraction. It is responsible for the decrease in reflection with larger numbers of drop-cast NP MLs in Fig. 3 and it greatly decreases the already small collected reflection from the top interface.

The reflected fraction predicted from the model shown in Fig. 3, assuming a 1 NP ML is at the interface, is ~50% larger than the experimental result (for 3 ML-equivalents drop-cast), and so it is generally consistent but not exactly the same. This signal is mostly due to the reflectance at the DEG/NP/heptane interface and so this difference is not surprising given the uncertainties in the effective medium models (which includes the uncertainty of the packing density of the NP cores in the ML (0.2910 in the model) and the difference in the actual and model real part of the refractive index of the NPs, including the possible decrease of the refractive index near the core surface), averaging due to inhomogeneities and imperfect coverage in the probed spot, uniformity of the NP layer at the interface meniscus, determination of the ML-equivalents for drop-casting, and so on.

The model and experimented reflected fraction indeed track each other for different numbers of NPs drop-cast above ~3 ML-equivalent drop-cast, which confirms that the NPs assembled at the liquid/liquid interface and essentially limited to 1 ML when at least 1 ML-equivalent of NPs was drop-cast.

To help corroborate this conclusion, after 1 ML-equivalent of NPs was drop-cast and the reflectance signal approached steady state, the NPs at the DEG/heptane interface were transferred onto a Si chip that was placed in the DEG in the center of the Petri dish and lifted up through the heptane layer, which would be essentially devoid of NPs if all had formed at the liquid/liquid interface. Scanning electron microscopy (SEM) analysis shows that ~90% of the chip area was covered with a single ML of hexagonal close-packed ordered NPs and ~10% were regions of thicker layers (Figure 4). After 3 ML-equivalents were drop-cast, ~80% of the regions were single NP ML. Figure 4 suggests that thicker regions might form at grain boundaries, either at the liquid/liquid interface or during and after the lift off process. Presuming these SEMs reflect the NP assembly at the interface (and not assembly afterwards, and this is not certain), this strengthens the conclusions of the reflection monitoring experiments that when 1 to 18 MLs were drop-cast, ~1 ML of NPs assembled at the liquid/liquid interface and the remaining NPs stayed in the heptane layer. Moreover, analogous studies of this system by the authors using SAXS monitoring and a cell designed specifically for SAXS, also indicate that 1 ML of these NPs form at the DEG/heptane interface after drop-casting 1 ML-equivalent or more, and this further substantiates the current conclusions using reflection monitoring.[20]

The experimental data in both Fig. 3 and Fig. S1 in the supplementary material suggest that the reflected fraction at the NP interface was not simply proportional to the number of ML-equivalents drop-cast for sub-monolayer (sub-ML) drop-casting (from 0 to 1 ML-equivalents), and that the reflectance may be first sub-linear and then super-linear (Fig. S3 in the supplementary material). Several factors may contribute to this, including how NP interface coverage varies with the number of drop-cast particles and how the reflectance at the DEG/NP/heptane interface varies with NP coverage.

The areal density of NPs at the DEG/heptane interface could be expected to increase with the number of drop-cast NPs and exponentially approach 1 ML of close-packed NPs, as in the Langmuir model of isothermal adsorption at a surface (Fig. S3 in the supplementary material). This model usually assumes a fixed partial pressure or density in the medium above the interface, and would need to be modified here because the total number of NPs at the interface and in the liquid medium above it is fixed here and not the density above the surface. However, the predicted surface coverage dependence changes little when this feature is included in the model. Moreover, the simple Langmuir model assumes the binding

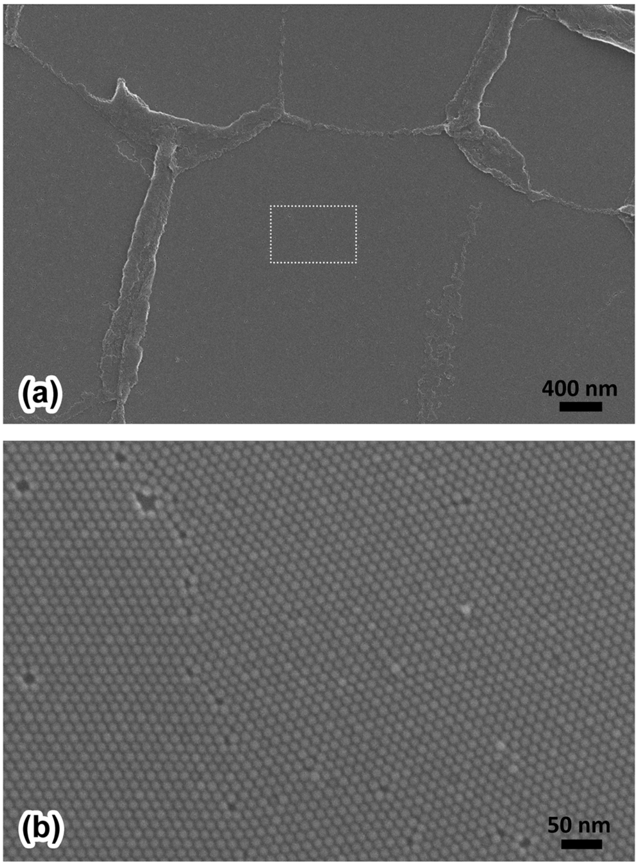

FIG. 4. Scanning electron micrographs of the NP layer at the DEG/heptane interface lifted on a Si surface, and then allowed to dry, with (b) being an expanded view of (a) in the white dotted box.

energy to the surface is independent of coverage. The plots in Fig. S3 in the supplementary material shows that the sub-ML surface coverage predicted by this model could track experiment (also in Fig. S3) if the binding energy of the NPs to the DEG/heptane interface depended on interface NP coverage, perhaps being proportional to it. This might happen if the local liquid interface near each NP changes as the NP coverage increases and the NP-NP distance decreases, causing stronger average NP binding to the liquid/liquid interface.

This discussion of sub-ML coverage has also presumed that the reflected fraction from the DEG/NP/heptane interface increases linearly with coverage up to 1 ML in the effective medium models; however, the scaling of such models at sub-ML coverages is not clear. Furthermore, if the liquid interface near each NP changes in the approach to close-packed NP coverage, as just noted, this would lead to more DEG and less heptane within the effective NP layer. So, the effective refractive index would increase (as in the models shown in Fig. S2) and the reflected fraction would increase super-linearly.

IV. CONCLUSIONS

Iron oxide NPs are seen to assemble at the DEG/heptane interface before the heptane solvent evaporates, and that this assembly self-limits to a single ML of NPs. In addition, this study has shown the value of using simple optical reflection near Brewster's angle to improve sensitivity by lessening the background interface reflection, to monitor NP MLs. In some ways, this optical method provides the same information as SAXS, but is simpler and less expensive, while being quite sensitive. It averages over a 2D region of a desired diameter, whereas SAXS integrates across a line (1D). Of course, optical reflectometry does not have many of the valuable capabilities of SAXS, such as determining NP ordering and separation, and when coupled with wide-angle x-ray scattering (WAXS), NP orientation.

SUPPLEMENTARY MATERIAL

See the supplementary material, which contains the results of additional experimental runs and of several effective medium-based reflection models, and observations and models for drop-casting sub-monolayer equivalents of NPs.

ACKNOWLEDGMENTS

Support was provided by the National Science Foundation (CBET-1603043), and to IGERT program of the National Science Foundation (DGE-1069240) for support of the REU program. The authors thank Sanat Kumar, Oleg Gang, Michal Lipson's group, Jason Cardarelli, and Lyuwen Fu for discussions and other help. The unpublished research cited here used the CMS 11-BM beamline and other resources of the National Synchrotron Light Source II (NSLS-II) and resources of the Center for Functional Nanomaterials, which are U.S. Department of Energy (DOE) Office of Science User Facilities operated for the DOE Office of Science by Brookhaven National Laboratory (BNL) under Contract No. DE-SC0012704. We thank Drs. Masafumi Fukuto, Ruipeng Li, and Kevin Yager at the BNL NSLS-II CMS 11-BM beamline for their assistance in that work.

REFERENCES

[1] V. Aleksandrovic, D. Greshnykh, I. Randjelovic, A. Fromsdorf, A. Kornowski, S. V. Roth, C. Klinke, and H. Weller, ACS Nano **2**, 1123 (2008).

[2] T. P. Bigioni, X. M. Lin, T. T. Nguyen, E. I. Corwin, T. A. Witten, and H. M. Jaeger, Nat. Mater. **5**, 265 (2006).

[3] C. Lu, D. Zhang, A. van der Zande, P. Kim, and I. P. Herman, Nanoscale **6**, 14158 (2014).

[4] D. Zhang, C. Lu, J. Hu, S. W. Lee, F. Ye, and I. P. Herman, J. Phys. Chem. C **119**, 10727 (2015).

[5] D. Zhang, J. Hu, K. M. Kennedy, and I. P. Herman, Langmuir **32**, 8467 (2016).

[6] P. Pieranski, Phys. Rev. Lett. **45**, 569 (1980).

[7] L. A. Girifalco and R. J. Good, J. Phys. Chem. **61**, 904 (1957).

[8] R. J. Good and E. Elbing, Ind. Eng. Chem. **62**, 54 (1970).

[9] A. Fortini, Phys. Rev. E **85**, 040401 (2012).

[10] B. P. Binks, Curr. Opin. Colloid Interface Sci. **7**, 21 (2002).

[11] M. Porus, P. Maroni, and M. Borkovec, Sens. Actuators B Chem. **151**, 250 (2010).

[12] M. Lublow and H. J. Lewerenz, Surf. Sci. **602**, 1677 (2008).

[13] J. R. Heath, C. M. Knobler, and D. V. Leff, J. Phys. Chem. B **101**, 189 (1997).

[14] S. Henrichs, C. P. Collier, R. J. Saykally, Y. R. Shen, and J. R. Heath, J. Am. Chem. Soc. **122**, 4077 (2000).

[15] P. P. Fang, S. Chen, H. Deng, M. D. Scanlon, F. Gumy, H. J. Lee, D. Momotenko, V. Amstutz, F. Cortés-Salazar, C. M. Pereira, and Z. Yang, ACS Nano **7**, 9241 (2013).

[16] T. Hyeon, S. S. Lee, J. Park, Y. Chung, and H. B. Na, J. Am. Chem. Soc. **123**, 12798 (2001).

[17] I. P. Herman, *Optical diagnostics for thin film processing* (Academic Press, New York, 1996), Chap. 9.
[18] G. A. Niklasson, C. G. Granqvist, and O. Hunderi, Appl. Opt. **20**, 26 (1981).
[19] J. E. Spanier and I. P. Herman, Phys. Rev. B **61**, 10437 (2000).
[20] J. Hu, E. W. C. Spotte-Smith, B. Pan, and I. P. Herman (unpublished).
[21] K. Kerl and H. Varchmin, J. Mol. Struct. **349**, 257 (1995).
[22] J. Rumble, *CRC handbook of chemistry and physics*, 99th ed. (CRC Press, Boca Raton, 2018).
[23] https://refractiveindex.info/, downloaded March 26, 2019.
[24] I. Z. Kozma, P. Krok, and E. Riedle, J. Opt. Soc. Am. B **22**, 1479 (2005).
[25] M. R. Querry, *Optical Constants, Contractor Report* (US Army Chemical Research, Development and Engineering Center (CRDC), Aberdeen Proving Ground, MD, 1985).